THE JOURNAL OF PHYSICAL CHEMISTRY C

Article

Cite This: J. Phys. Chem. C 2019, 123, 8813−8817

pubs.acs.org/JPCC

Crucial Role of Metal Surface Morphology in Photon Emission from a Tunnel Junction at Ambient Conditions

Vitaliy A. Shkoldin,*[,†,‡] Dmitry V. Permyakov,*[,†] Konstantin S. Ladutenko,[†] Mikhail V. Zhukov,[†,§] Aleksandr A. Vasiliev,[‡] Alexander O. Golubok,[†,§] Alexander V. Uskov,[†,∥] Alexey D. Bolshakov,[‡] Andrey A. Bogdanov,[†] Anton K. Samusev,[†] and Ivan S. Mukhin[†,‡]

[†]ITMO University, St. Petersburg 197101, Russia

[‡]St. Petersburg Academic University, St. Petersburg 194021, Russia

[§]Institute for Analytical Instrumentation RAS, St. Petersburg 198095, Russia

[∥]P. N. Lebedev Physical Institute, Russian Academy of Sciences, Moscow 119991, Russia

Supporting Information

ABSTRACT: In this paper, we study light emission from a tunnel contact between the Au film on a glass substrate and the Au-coated tungsten probe of the scanning tunneling microscope at ambient conditions. We investigate the dependence of the intensity of the collected optical signal on the film surface morphology, namely, on geometrical parameters of nanometer-scale gold grains (islands) constituting the film. We reveal that the magnitude of inelastic tunnel current and thus photon emission intensity increase both with the decrease of island height and the increase of island width. We show that the difference in the optical emission intensity could reach 4 orders of magnitude for poly- and monocrystalline (atomically flat) samples. The observed phenomena are explained with dependence of the effective area of a tunnel contact on the grain aspect ratio. The obtained results demonstrate the crucial role of the sample morphology in influencing the efficiency of photon emission from the tunnel junction.

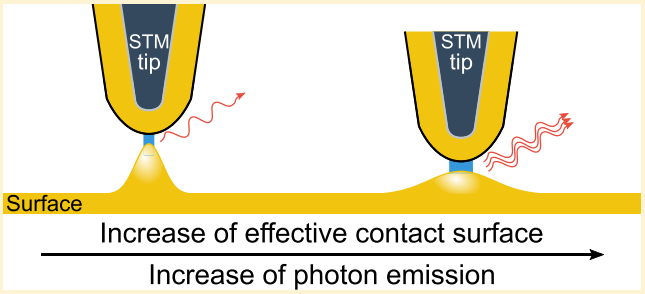

INTRODUCTION

The ever-growing rate of digital data processing leads to continuous improvement of computational devices aimed at enhancement of their performance and decrease of energy consumption. Modern computational devices are based on traditional integrated circuits with data transfer via electronic signal processing. Performance of these devices is close to the theoretical limit nowadays. One of the promising ways to overcome the existing limitations is transition to the optical platform with use of photonic integrated circuits, which may provide an increase of operating frequencies along with the reduced Joule heating.

The optical pathway used to transfer information between data centers has already proven its robust performance. In 2009, this technology was awarded the Nobel prize.[1] Despite fast development of some perspective optical technologies (e.g., Li−Fi), the optical data processing on a chip is still on its early stage of evolution.

Fabrication of the integrated optoelectronic circuits involves development of many components including logic elements, amplifiers, receivers, waveguides, and electrically driven localized photonic and plasmonic emitters. Semiconductor lasers with Fabry−Perot resonators, microdiscs, and Fano lasers[2] are potential candidates for the latter role. However, in these devices, the resonator *Q*-factor becomes rather low when dimensions go below the scale of an operating wavelength. As a result, this leads to the increase of the laser threshold.[3] Moreover, these systems are not applicable for development of the single-photon emitters used in quantum communication systems. Thereby, traditional laser emitters do not satisfy new IT circuit requirements.

One of the promising ways to develop submicron-sized photonic emitters is the use of a tunnel electrical contact. Lambe and McCarthy demonstrated[4] for the first time the effect of light emission during inelastic electron tunneling in a planar metal−dielectric−metal structure with a thin potential barrier. According to the results of several theoretical and experimental works,[5] light emission in this system is related to quantum oscillations of the tunnel current. This type of emission is broadband, but in the single-electron approximation, the resulting photon energy is limited with a potential energy determined with the bias applied to the tunnel gap.[5]

An enhanced photon emission in a tunnel contact between a metal tip of scanning tunneling microscope (STM) and a metal layer was demonstrated by Gimzewski et al.[6] This effect occurs because of the increase of the local density of optical states in

Received: November 21, 2018
Revised: March 7, 2019
Published: March 11, 2019

DOI: 10.1021/acs.jpcc.8b11271
J. Phys. Chem. C 2019, 123, 8813−8817

the tunnel gap under the STM probe. In this system, the tunnel gap has a size of few nanometers and can be considered as a subwavelength photonic source (including the potential to operate in the single-photon emission regime[7]) driven electrically. Still, the quantum yield of photon emission is rather low with an efficiency of 10^{-6} to 10^{-4}.[8]

An optical subwavelength nanoantenna can be placed in the tunnel gap to enhance emission probability.[9] Experimentally, amplification of electroluminescence in a planar metal structure with a spherical Au nanoantenna in the tunnel gap was demonstrated in ref 10. The tunnel gap between the STM tip and planar metal interface can also be used as a point source of surface plasmon polaritons.[4] It has been shown theoretically[11] that introduction of the metal nanoantenna beneath the STM probe tip should lead to resonant increase of the quantum yield of this process by more than 2 orders of magnitude which is accompanied by narrowing of the optical emission spectrum.

In order to study all those effects, it would be very useful to be capable of carrying out experiments on light emission from the tunnel contact in STM at ambient conditions. This approach should make these studies simpler and faster.

In this work, we study the emission rate from the tunnel gap between the STM probe and a substrate covered with the Au film and demonstrate the influence of the film surface properties on photon emission process efficiency. We show experimentally that reduction of the surface roughness leads to significant increase in the intensity of emission from the STM contact. Investigation of the surface morphology effects on the emission is extremely important on the way to the development of efficient nanoscale light sources.

EXPERIMENTAL SETUP AND SAMPLES

In this work, the tunnel gap was implemented between the STM probe and a thin Au film deposited on a glass substrate (Figure 1). The probe was fabricated from a 150 μm tungsten wire using electrochemical etching in KOH solution followed by thermal evaporation of a ~30 nm thick Au layer and Cr adhesive underlayer on the probe tip. The tip characteristic radius of about 100 nm was controlled by means of scanning electron microscopy (see the inset in Figure 1).

The second contact of the tunnel junction was made by deposition of gold films (15−50 nm) on 150 μm glass substrates covered with a chromium adhesive underlayer (1−2 nm). Varying the technological parameters of the deposition process, we synthesized the gold films with different thickness and morphology.

STM based on AIST-NT Combiscope with integrated inverted optical microscope was used to study light emission from the tunnel junction. The emission was captured by Olympus 100× NA = 0.95 objective from the substrate side and detected by an ID Quantique ID120 single-photon avalanche photodiode unless otherwise specified.

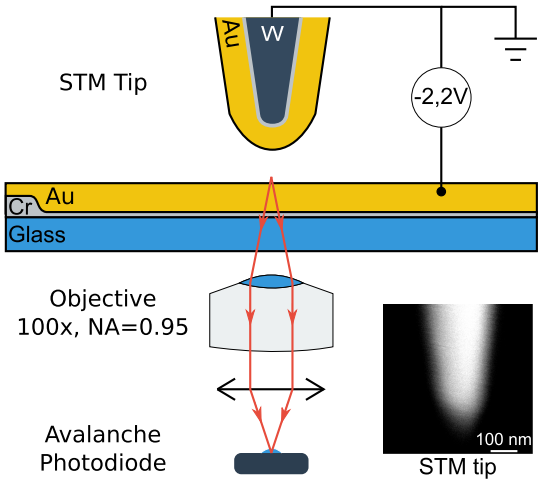

Figure 1. Scheme of the experimental setup. STM with an integrated inverted optical microscope. Tunnel current flows between the tip of the STM probe and Au film deposited on a glass substrate. The inset shows the scanning electron microscopy image of a typical STM tip used.

EXPERIMENTAL RESULTS AND MODELING

Light emission from a tunnel junction takes place if a bias (V_b) is applied to its contacts. During the electron tunneling, elastic and inelastic processes occur. In the first case, the electron's energy remains the same after the tunneling through the potential barrier. In the second case, the energy is lost during the tunneling. This energy could be transferred to plasmon excitation and photon emission. The scheme of the tunnel junction band diagram and spectral density of temporal fluctuation of tunnel current defining the emission spectrum,[10] which can be expressed as $C(\omega) = (eV_b - \hbar\omega)$, where ω is photon frequency, are presented in Figure 2. The photon

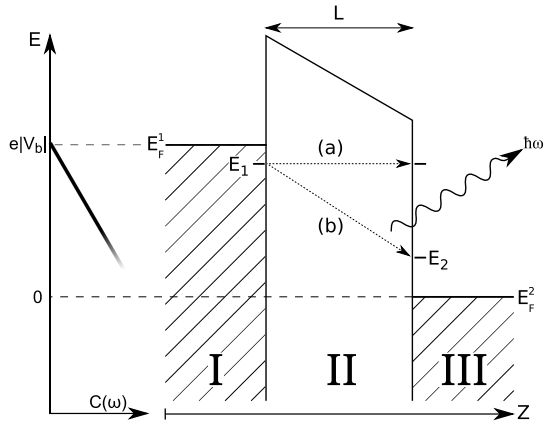

Figure 2. Band diagram of a tunnel junction between two metals: I—probe with Au-coated tip, II—potential barrier region, III—Au film, E_F^1, E_F^2—Fermi levels in regions I and III, correspondingly, L—gap between the probe tip and the sample, E_1, E_2—electron energies before and after the tunneling, and V_b—applied bias. Process (a) corresponds to elastic tunneling and (b) inelastic tunneling with partial electron energy loss.

emission spectrum of a tunnel junction depends on several parameters, including contact materials and applied bias.[12] In the single-particle process, photon energy is limited by the bias value V according to the relation: $\hbar\omega \leq |eV|$[4]. Hence, to obtain visible range emission, we need to apply (1.5−3) V bias.

Our study was intentionally conducted at ambient conditions. Normally, the sample and tip surface is covered with a thin (~1 nm) water layer and when the tip approaches the surface, a meniscus appears in between.[13] When the applied bias value exceeds 1.23 V (the standard electrochemical potential for water electrolysis), water molecules decompose with subsequent formation of ions.[14] Conse-

DOI: 10.1021/acs.jpcc.8b11271
J. Phys. Chem. C 2019, 123, 8813−8817

quently, current between the Au film and the tip has two contributions: tunnel current and ionic current of electrochemical nature. Photon emission relates to the tunnel current fluctuations, while occurrence of the ionic current is a parasitic effect that negatively affects the tunnel contact stability.[8]

Three modes of STM operating at ambient conditions and relatively high applied bias (above 1.23 V) can be distinguished:[8] "stable current" mode, "unstable current" mode providing fluctuations of the tunnel current, and "saturation" mode with oscillations of the probe and high peaks of current. In the latter mode, the system promotes fast approach of the probe to the sample and when the current flow occurs, the STM feedback system immediately breaks the contact moving the probe off the sample. As a result, oscillations of the gap occur resulting in the tunnel current fluctuations, while the total current value remains. It was demonstrated that the "saturation" regime provides maximum photon emission efficiency.[8] In our experiments, the maintained mean current value was 165 nA with an applied bias value of 2.2 V, and the probe oscillation frequency was 52 Hz. The voltage was applied to the substrate that is denoted as a value of −2.2 V shown in Figure 1.

Prior to photon emission studies, the surface morphology of the samples was investigated with atomic force microscopy. The obtained images (see the Supporting Information) demonstrate the topography of the film surface with specific grain geometry for each of the samples. Using standard tools, we calculate the roughness of the surface (the root mean square of surfaces, rms (σ)) and the autocorrelation length of grains' image (ξ).[15,16] These parameters could be associated with the average height and the average diameter of grains, respectively. Parameters of the samples morphology are average metal film thickness (h_{Cr}, h_{Au}), the autocorrelation length of grain's image (ξ), the roughness of the surface (rms), (σ) and their aspect ratio ($A = \sigma/\xi$) are presented in Table 1.

Table 1. Parameters of the Samples and Experimental Data[a]

#	h_{Cr} (nm)	h_{Au} (nm)	σ (nm)	ξ (nm)	A	I_n (%)
1	5.6	47	2.22	24.7	0.090	0.15
2	6.1	43	2.55	32.4	0.075	0.44
3	4.0	27	1.59	26.6	0.060	2.65
4	4.6	16	1.27	33.2	0.038	3.76
5	2.7	26	0.91	31.7	0.029	100
SC[b]		300	→0	→∞	→0	900[c]

[a]h_{Cr}, h_{Au}—average metal film thickness, σ and ξ—the roughness of the surface (the root-mean-square roughness, rms) and the autocorrelation length of grains, respectively, and $A = \sigma/\xi$—aspect ratio. [b]Monocrystalline Au. [c]The measured value obtained with the lens installed at an angle of 25° relative to the substrate surface and normalized over sample #5 emission intensity measured with the same lens setup.

In order to retrieve the average thickness of gold and chromium layers with high precision, we have measured the transmission spectrum of each sample (see Figure 3a). The experimental data were approximated with the use of Cr and Au layer thickness as fitting parameters. The simulations (black solid curves in Figure 3a) were carried out in the TFCalc software package using the transfer-matrix method.[17] Frequency dispersion of these materials were taken from ref 18.

Results of numerical modeling allow to state that material properties of the Au film and Cr sublayer do not depend on the deposition technique parameters due to the fact that the spectra obtained experimentally are approximated with high accuracy in a broad range of wavelengths using the transfer-matrix method with only two fitting parameters, namely, thicknesses of Au and Cr layers.

As a result, we evaluated thicknesses of the metal films for each of the sample with high accuracy (see Table 1). Notably, despite only 2 nm difference in the total film thickness between samples 3 and 5, their transmission spectra differ sufficiently. Resonant enhancement of the transmission near a wavelength of 530 nm relates to dispersion features of the Au dielectric function. According to the experimental data, the transmission coefficient mainly depends on the total thickness of the deposited metal layers, rather than on their surface morphology (see Table 1).

Figure 3b shows spectral dependencies of light emission of the vertical electric dipole toward the substrate side simulated for samples #1−#5, reproducing experimental geometry (for more details, see the Supporting Information). The obtained spectra show good qualitative agreement with the case of normal-incidence transmission (Figure 3a). This allows us to use the measured transmissivity of the substrate to estimate the relative emission efficiency for different samples.

In our experimental series, we used the same STM probe and feedback system parameters to study each of the samples. To verify reproducibility of the experimental data at the first step, we measured emission of sample 5 (providing maximum intensity). Then, we studied samples from 1 to 4 and repeated the experiment with sample 5 again. The latter measurement demonstrated good proximity to the initial results, allowing us to conclude that the probe was not modified discernibly during the experimental runs. The normalized value of the measured mean emission intensity I_n is presented in Table 1. The measured emission intensity was normalized over the measured transmission coefficient at a wavelength of 740 nm (see Figure 3a), which is the central wavelength of emission spectra of the Au−Au STM tunnel contact observed in a similar experimental geometry.[19]

The obtained data presented in Table 1 demonstrate correlation between the Au film surface morphology and the emission intensity. The increase of the surface grains' lateral dimension (ξ) led to rise of the emission intensity. Decrease of the grains' mean height (σ) had similar influence. From this, one can assume that the emission intensity strongly depends on the grains' aspect ratio $A = \sigma/\xi$: the intensity dramatically increases with decrease of the aspect ratio.

Additionally, we investigated the emission from the 300 nm thick monocrystalline Au film, representing the utmost case as parameter A tends to zero. In this case, the substrate is practically opaque, so the emission was captured by means of long focus lens placed above the sample aside the STM probe at an angle of 25° relative to the substrate surface. To provide accurate comparison of the experimental results obtained with the two geometries, the emission intensity registered from monocrystalline gold was normalized over the intensity of sample 5 emission measured with the same long focus lens. The experimental data demonstrate that the emission efficiency can further be increased by an order of magnitude using the monocrystalline Au sample (see Table 1).

DISCUSSION

According to the data presented in Table 1, photon emission from the STM tunnel gap can be tailored in a broad range:

DOI: 10.1021/acs.jpcc.8b11271
J. Phys. Chem. C 2019, 123, 8813−8817

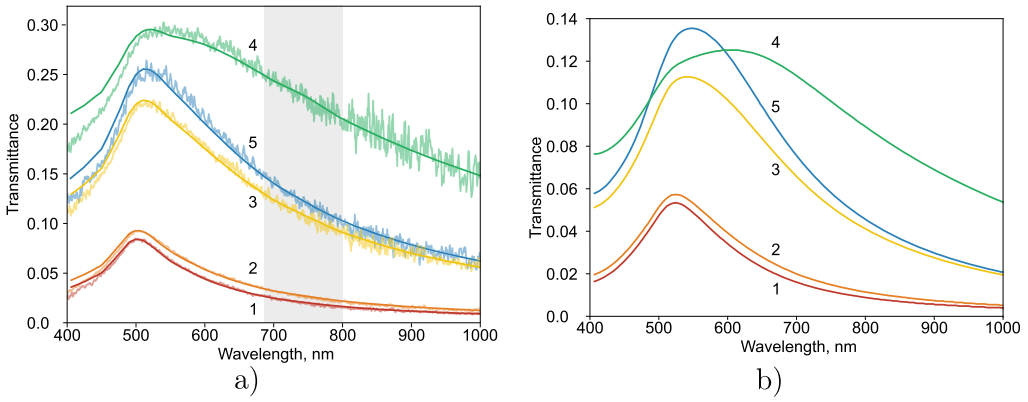

Figure 3. (a) Measured normal-incidence transmission spectra of samples from 1 to 5 (thin curves). Simulated transmission spectra fitted to the experimental data by varying Au and Cr layer thicknesses (thick curves). (b) Simulated transmission spectrum obtained with the excitation by a vertical point dipole placed in the vicinity of the sample surface. The numerical aperture of the capturing objective lens is taken into account. The curve numbering correspond to Table 1.

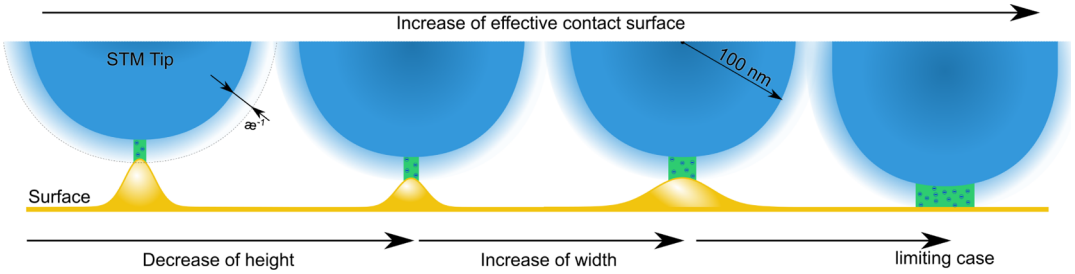

Figure 4. Influence of the shape of the Au island on the effective tunnel contact.

with the same mean total current, the emission intensity can vary by almost 4 orders of magnitude depending on the sample, while morphological parameters are only slightly varied.

Comparison of the results obtained with samples 3 and 5 shows that despite almost the same thickness of the Au film and moderate (two times) change in the aspect ratio, the emission intensity differed in ~37 times.

The obtained difference in emission can be related to both variation of the tunnel current and to various emission output efficiencies from the gap due to the Purcell factor.[20] Good agreement between far-field transmission spectra (Figure 3a) with the emission spectra of the point vertical dipole placed next to the substrate (Figure 3b) supports the fact that in the system under study, the Purcell effect is negligible. Therefore, the variation of emission intensity is governed mainly by the change of tunnel current.

It is known that the tunnel current density depends exponentially on the gap size. One of the parameters of this exponential dependence is electron wave function decay length: $\kappa^{-1} = [2m(eV_b - \varepsilon_F)]^{-1/2}$, where m is the electron mass, ε_F is the Fermi level of the electron in metal.[21] The maximum current value is obtained with a zero gap, which corresponds to a short circuit.

In earlier work,[22] it was demonstrated that the tunnel current (as well as short circuit current) between the two metals is proportional to the contact effective area S. If one of the contacts has Gaussian shape islands with height Z_{grain} (equivalent to σ) and half-width diameter D_{grain} (equivalent to ξ), this area can be expressed as $S \propto (D_{grain}/\kappa Z_{grain})^2 = (\kappa A)^{-2}$, being inversely proportional to the grain aspect ratio.

Figure 4 schematically shows how contact effective area increases with the decrease of the grain height (Z_{grain}) and with the increase of its diameter D_{grain}. It is worth noting that the model is correct, while the grain size is much smaller than the probe tip radius. In the case of a smooth sample surface of the monocrystalline Au film, the major impact on the contact area has the shape of the probe tip.

The considerations above allow us to explain the experimental results presented in Table 1. The decrease of the aspect ratio A (see samples form #1 to #5) leads to the increase of the tunnel current along with increase of the emission intensity by almost 3 orders of magnitude. When the probe approaches the atomically flat surface of the monocrystalline Au film, the emission efficiency is only limited by the tip curvature and increases by 1 order of magnitude as compared to a slightly rough surface.

As demonstrated in the pioneering work by Lambe and McCarthy,[4] as well as in later works, for example,[9] when the bias is applied to the planar metal−insulator−metal tunnel contact, the photon emission is accompanied with effective generation of surface plasmon polaritons. Transition of a surface wave into a volume wave occurs at scattering centers on the surface, for example, surface roughness. From this point of view, the photon emission should be substantially less effective on the atomically flat surface. On the other hand, as shown in ref 22, flat surfaces of the tunnel junction stimulate larger tunneling current (at the same distance between the probe and the substrate), and as a result, a larger amount of energy transforms into the photon emission. Our experimental data clearly show that in the STM oscillation mode at ambient conditions, the second mechanism prevails because more efficient emission is observed in the case of a smoother surface.

DOI: 10.1021/acs.jpcc.8b11271
J. Phys. Chem. C 2019, 123, 8813−8817

CONCLUSIONS

We have studied photon emission from the tunnel gap between the Au-coated STM probe and Au films with different morphologies of interfaces. We have shown experimentally that the decrease of height and increase of width of Au grains both lead to sufficient increase of photon emission from the tunnel contact. In the same STM regime, one could tailor the emission efficiency in a broad range covering 4 orders of magnitude by alternating the surface morphology. The obtained phenomenon is explained via strong influence of the surface geometry on effective area of the tunnel contact which is inversely proportional to square of the grain aspect ratio.

We therefore conclude that the improvement of the sample surface quality at the scale of nanometers or even angstroms is crucial and can be employed for the enhancement of photon emission intensity from a tunnel gap. Because of the low quantum yield of the emission in the tunneling process, our results have an important value for the development of effective single-photon emitters—basic optoelectronic components.

ASSOCIATED CONTENT

Supporting Information

The Supporting Information is available free of charge on the ACS Publications website at DOI: 10.1021/acs.jpcc.8b11271.

Calculation methods and atomic force microscopy images (PDF)

LaTeX sources of the Supporting Information (ZIP)

AUTHOR INFORMATION

Corresponding Authors

*E-mail: shkoldin@corp.ifmo.ru (V.A.S.).
*E-mail: d.permyakov@metalab.ifmo.ru (D.V.P.).

ORCID

Vitaliy A. Shkoldin: 0000-0002-1014-5401
Dmitry V. Permyakov: 0000-0003-2708-9140
Alexander V. Uskov: 0000-0001-8816-4103
Andrey A. Bogdanov: 0000-0002-8215-0445
Anton K. Samusev: 0000-0002-3547-6573

Notes

The authors declare no competing financial interest.

ACKNOWLEDGMENTS

The authors thank Artur Gleym and Semen Smirnov for assistance in experimental measurements. The authors are also grateful to Robert A. Suris for fruitful discussions. This work was carried out with the support of the Russian Science Foundation (Grant 17-19-01532).

REFERENCES

(1) Kao, C. K.; Boyle, W. S.; Smith, G. E. Transmission of Light in Fiber for Optical Communication. *Science* **2011**, *7*, 109.

(2) Yu, Y.; Xue, W.; Semenova, E.; Yvind, K.; Mork, J. Demonstration of a self-pulsing photonic crystal Fano laser. *Nat. Photonics* **2017**, *11*, 81.

(3) Ustinov, V.; Zhokov, A.; Press, O. U.; Zhukov, A.; Egorov, A.; Maleev, N. *Quantum Dot Lasers*; Oxford Science Publications; Oxford University Press, 2003.

(4) Lambe, J.; McCarthy, S. L. Light emission from inelastic electron tunneling. *Phys. Rev. Lett.* **1976**, *37*, 923.

(5) Schneider, N. L.; Schull, G.; Berndt, R. Optical probe of quantum shot-noise reduction at a single-atom contact. *Phys. Rev. Lett.* **2010**, *105*, 026601.

(6) Gimzewski, J. K.; Sass, J. K.; Schlitter, R. R.; Schott, J. Enhanced photon emission in scanning tunnelling microscopy. *Europhys. Lett.* **1989**, *8*, 435.

(7) Zhang, L.; et al. Electrically driven single-photon emission from an isolated single molecule. *Nat. Commun.* **2017**, *8*, 580.

(8) Rogez, B.; Cao, S.; Dujardin, G.; Comtet, G.; Moal, E. L.; Mayne, A.; Boer-Duchemin, E. The mechanism of light emission from a scanning tunnelling microscope operating in air. *Nanotechnology* **2016**, *27*, 465201.

(9) Parzefall, M.; Bharadwaj, P.; Novotny, L. *Springer Series in Solid-State Sciences*; Springer International Publishing, 2017; pp 211−236.

(10) Kern, J.; Kullock, R.; Prangsma, J.; Emmerling, M.; Kamp, M.; Hecht, B. Electrically driven optical antennas. *Nat. Photonics* **2015**, *9*, 582.

(11) Bigourdan, F.; Hugonin, J.-P.; Marquier, F.; Sauvan, C.; Greffet, J.-J. Nanoantenna for electrical generation of surface plasmon polaritons. *Phys. Rev. Lett.* **2016**, *116*, 106803.

(12) Berndt, R.; Gimzewski, J. K.; Johansson, P. Inelastic tunneling excitation of tip-induced plasmon modes on noble-metal surfaces. *Phys. Rev. Lett.* **1991**, *67*, 3796.

(13) Gómez-Monivas, S.; Sáenz, J. J.; Calleja, M.; García, R. Field-induced formation of nanometer-sized water bridges. *Phys. Rev. Lett.* **2003**, *91*, 056101.

(14) Senftle, F. E.; Grant, J. R.; Senftle, F. P. Low-voltage DC/AC electrolysis of water using porous graphite electrodes. *Electrochim. Acta* **2010**, *55*, 5148−5153.

(15) Gredig, T.; Silverstein, E. A.; Byrne, M. P. Height-Height Correlation Function to Determine Grain Size in Iron Phthalocyanine Thin Films. *J. Phys.: Conf. Ser.* **2013**, *417*, 012069.

(16) Stone, V. W.; Jonas, A.; Nysten, B.; Legras, R. Roughness of free surfaces of bulk amorphous polymers as studied by x-ray surface scattering and atomic force microscopy. *Phys. Rev. B: Condens. Matter Mater. Phys.* **1999**, *60*, 5883.

(17) TFCalc—Software for the Design and Manufacture of Optical Thin Film Coatings. http://www.sspectra.com/ (Accessed 1 March 2019).

(18) Olmon, R. L.; Slovick, B.; Johnson, T. W.; Shelton, D.; Oh, S.-H.; Boreman, G. D.; Raschke, M. B. Optical dielectric function of gold. *Phys. Rev. B: Condens. Matter Mater. Phys.* **2012**, *86*, 235147.

(19) Wang, T.; Boer-Duchemin, E.; Zhang, Y.; Comtet, G.; Dujardin, G. Excitation of propagating surface plasmons with a scanning tunnelling microscope. *Nanotechnology* **2011**, *22*, 175201.

(20) Purcell, E. M. *Confined Electrons and Photons*; Springer, 1995; pp 839.

(21) Harrison, W. A. Tunneling from an independent-particle point of view. *Phys. Rev.* **1961**, *123*, 85.

(22) Krylov, M.; Suris, A. Electron tunneling through layers with statistically rough surfaces. *Zh. Eksp. Teor. Fiz.* **1985**, *88*, 2204−2221 Retrieved from http://www.jetp.ac.ru/cgi-bin/dn/e_061_06_1303.pdf .

DOI: 10.1021/acs.jpcc.8b11271
J. Phys. Chem. C 2019, 123, 8813−8817